Wind and Structures, *Vol. 21, No. 1 (2015) 41-61*
DOI: http://dx.doi.org/10.12989/was.2015.21.1.041

Flutter stability of a long-span suspension bridge during erection

Yan Han[1a], Shuqian Liu[1], C.S. Cai[*1,2] and Chunguang Li[1]

[1]*School of Civil Engineering and Architecture, Changsha University of Science & Technology, Changsha, China, 410004*
[2]*Department of Civil and Environmental Engineering, Louisiana State University, Baton Rouge, Louisiana, USA, LA 70803*

(Received December 6, 2014, Revised April 6, 2015, Accepted April 20, 2015)

Abstract. The flutter stability of long-span suspension bridges during erection can be more problematic and more susceptible to be influenced by many factors than in the final state. As described in this paper, numerical flutter stability analyses were performed for the construction process of Zhongdu Bridge over Yangtze River using the commercial FE package ANSYS. The effect of the initial wind attack angle, the sequence of deck erection, the stiffness reduction of stiffening girders, the structural damping, and the cross cables are discussed in detail. It was found that the non-symmetrical sequence of deck erection was confirmed to be aerodynamically favourable for the deck erection of long-span suspension bridges and the best erection sequence should be investigated in the design phase. While the initial wind attack angle of -3^o is advantageous for the aerodynamic stability, $+3^o$ is disadvantageous compared with the initial wind attack angle of 0^o during the deck erection. The stiffness reduction of the stiffening girders has a slight effect on the flutter wind speed of the suspension bridge during erection, but structural damping has a great impact on it, especially for the early erection stages.

Keywords: long-span suspension bridges; flutter stability; deck erection; finite element (FE) model; ANSYS

1. Introduction

The assessment of the aerodynamic behavior of long-span bridges during the design process is essential. The collapse of the Old Tacoma Narrows Bridge under a relatively low wind speed highlighted the importance of sound aerodynamic design against bridge flutter. Flutter that occurs when the critical wind speed is exceeded is a self-induced periodic motion with divergent amplitudes leading to the destruction of the structure. Compared to a bridge in service conditions, the overall stiffness of a bridge under erection is greatly reduced, and consequently it becomes very susceptible to the dynamic wind action. Although the period of erection is relatively short and the design wind speed can be reduced, however, the flutter wind speed can also be very low due to the flexibility of the structure, especially at the early stages of construction. Thus, it is now

∗Corresponding author, Professor, E-mail: cscai@lsu.edu
[a] Associate Professor, E-mail: ce_hanyan@163.com

http://www.techno-press.org/?journal=was&subpage=8 ISSN: 1226-6116 (Print), 1598-6225 (Online)

commonly believed that, regarding wind stability, construction conditions are often less favorable than the final state.

The aerodynamic stability of long-span suspension bridges under erection conditions particularly has been an important engineering issue, which has attracted considerable attention during the past few decades (Brancaleoni and Brotton 1981, Brancaleoni 1992, Larsen 1993, 1995, Tanaka *et al*. 1996, 1999, Yoneda *et al*. 1998, Ge and Tanaka 2000, Liu *et al*. 2000, Diego Cobo del Arco 2001, Zhang 2004, 2006). These investigations have found some important factors governing the aerodynamic stability of suspension bridges under construction including dynamic characteristics, structural stiffness and damping, the influence of finite deck length, the nonlinear effects of wind-structure interactions, erection sequence, the provision of eccentric mass, dampers, and cross cables. However, these aerodynamic stability analyses were mainly based on the special purpose FE packages developed to tackle flutter analysis of bridges or on the aeroelastic wind tunnel tests, which are typically unavailable for the bridge designers and engineering practitioners. While the commercial finite element (FE) packages such as ANSYS and ADINA are usually available for practicing engineers, the commercial FE packages cannot be directly used for flutter analysis of long-span bridges due to the lack of the capability of calculating the motion-dependent wind loads. Some efforts (Hua *et al*. 2007, Han 2007, Chen *et al*. 2009) have been made to provide an alternative way for the bridge designers and engineering practitioners for the flutter and buffeting analysis of long-span bridges by using ANSYS.

The present paper focuses its attention on the flutter stability of a long-span suspension bridge during erection, the Zhongdu Bridge over Yangtze River with a central span 600 m and a stiffening box girder with a streamlined shape. This type of suspension bridge typically does not have flutter problem. However, the meteorological conditions of the Zhongdu Bridge over Yangtze River are really complicated and the basic wind speed is very high. Hence, the designers required an evaluation of the flutter performance by section model tests and finite element analysis. For this the evolution of the fundamental vibration frequencies following different erection sequences has been produced and compared, to understand how the dynamic properties vary during the erection process. Flutter analysis was then performed by using ANSYS (Hua *et al*. 2007, Han 2007, Chen *et al*. 2009) based on the experimentally-determined flutter derivatives (Chen 2013). Both the symmetrical and non-symmetrical deck erection sequences were analyzed to find the optimized erection sequence. The effect of the initial wind attack angle, the stiffness reduction of stiffening girders, structural damping, and the cross cables under erection are discussed.

2. Aerodynamic stability analysis using ANSYS

The equation of motion of a bridge in the smooth flow can be expressed as

$$\mathbf{M}\ddot{\mathbf{q}} + \mathbf{C}\dot{\mathbf{q}} + \mathbf{K}\mathbf{q} = \mathbf{F}_{se} \tag{1}$$

where $\mathbf{M}$, $\mathbf{C}$ and $\mathbf{K}$ are the global mass, damping and stiffness matrices, respectively; $\mathbf{q}$, $\dot{\mathbf{q}}$ and $\ddot{\mathbf{q}}$ represent the nodal displacement, velocity and acceleration vectors, respectively; and $\mathbf{F}_{se}$ denotes the vector of the nodal aeroelastic forces.

Self-excited lift force L_{se}, drag force D_{se} and pitching moment M_{se} per unit length are defined as (Scanlan 1978, Jain *et al.* 1996)

$$L_{se}=\rho U^2 B\left[KH_1^*\frac{\dot{h}_b(x,t)}{U}+KH_2^*\frac{B\dot{\alpha}_b(x,t)}{U}+K^2H_3^*\alpha_b(x,t)+K^2H_4^*\frac{h_b(x,t)}{B}+KH_5^*\frac{\dot{p}_b(x,t)}{U}+K^2H_6^*\frac{p_b(x,t)}{B}\right] \quad (2a)$$

$$D_{se}=\rho U^2 B\left[KP_1^*\frac{\dot{p}_b(x,t)}{U}+KP_2^*\frac{B\dot{\alpha}_b(x,t)}{U}+K^2P_3^*\alpha_b(x,t)+K^2P_4^*\frac{p_b(x,t)}{B}+KP_5^*\frac{\dot{h}_b(x,t)}{U}+K^2P_6^*\frac{h_b(x,t)}{B}\right] \quad (2b)$$

$$M_{se}=\rho U^2 B^2\left[KA_1^*\frac{\dot{h}_b(x,t)}{U}+KA_2^*\frac{B\dot{\alpha}_b(x,t)}{U}+K^2A_3^*\alpha_b(x,t)+K^2A_4^*\frac{h_b(x,t)}{B}+KA_5^*\frac{\dot{p}_b(x,t)}{U}+K^2A_6^*\frac{p_b(x,t)}{B}\right] \quad (2c)$$

in which ρ is the air density; U is the mean wind velocity; B is the bridge deck width; $K=\omega B/U$ is the reduced circular frequency; H^*_i, P^*_i and A^*_i (i=1 to 6) are the aerodynamic derivatives related to the vertical, lateral, and torsional directions, respectively; $h_b(x,t)$, $p_b(x,t)$, and $\alpha_b(x,t)$ are the vertical, lateral, and torsion displacements of the bridge, respectively; and a dot superscript denotes the derivative with respect to the time.

In finite element analysis, if distributed forces are converted into equivalent nodal loadings acting at the member ends, the aeroelastic forces for element e can be expressed in terms of nodal displacement and nodal velocity as

$$\mathbf{F}^e_{ae}=\mathbf{K}^e_{ae}\mathbf{q}^e+\mathbf{C}^e_{ae}\dot{\mathbf{q}}^e \quad (3)$$

where $\mathbf{K}^e_{ae}$ and $\mathbf{C}^e_{ae}$ represent the local aeroelastic stiffness and damping matrices for element e, respectively; $\mathbf{q}^e=\{q_1 \quad q_2 \quad \ldots \quad q_{12}\}^T$ is the displacement vector of the element e with X_e, Y_e and Z_e being the axial, lateral and vertical coordinates, respectively, as shown in Fig. 1. Similar to the general procedures in formulating element mass matrix, either a lumped or consistent formulation can be used to derive the element aeroelastic stiffness and damping matrices (Namini 1991, Cai *et al*. 1999a). Chen and Han (2007) found that the flutter limit speed by using the lumped formulation is lower than that by using the consistent formulation, which is conservative. In this study, the lumped formulation was adopted and the expressions of $\mathbf{K}^e_{ae}$ and $\mathbf{C}^e_{ae}$ are expressed as

$$\mathbf{K}^e_{ae}=\begin{bmatrix}\mathbf{K}^e_{ae1} & 0\\ 0 & \mathbf{K}^e_{ae1}\end{bmatrix}, \qquad \mathbf{C}^e_{ae}=\begin{bmatrix}\mathbf{C}^e_{ae1} & 0\\ 0 & \mathbf{C}^e_{ae1}\end{bmatrix} \quad (4)$$

in which

$$\mathbf{K}^e_{ae1}=a\begin{bmatrix}0&0&0&0&0&0\\0&P_4^*&P_6^*&BP_3^*&0&0\\0&H_6^*&H_4^*&BH_3^*&0&0\\0&BA_6^*&BA_4^*&B^2A_3^*&0&0\\0&0&0&0&0&0\\0&0&0&0&0&0\end{bmatrix}, \quad \mathbf{C}^e_{ae1}=b\begin{bmatrix}0&0&0&0&0&0\\0&P_1^*&P_5^*&BP_2^*&0&0\\0&H_5^*&H_1^*&BH_2^*&0&0\\0&BA_5^*&BA_1^*&B^2A_2^*&0&0\\0&0&0&0&0&0\\0&0&0&0&0&0\end{bmatrix} \quad (5)$$

where $a=\rho U^2K^2L_e/2$ and $b=\rho UBKL_e/2$; and L_e is the length of element e.

Hua *et al*. (2007) developed a hybrid finite element model that uses *Matrix27* to model the flutter-derivative-based aeroelastic forces in ANSYS, and used it for flutter analysis in the frequency domain. The user-defined element in ANSYS, *Matrix27,* is a versatile element with two

nodes each having six degrees of freedom, and its local coordinate system is parallel to the global coordinate system. Note that one *Matrix27* element can only model either an aeroelastic stiffness component or an aeroelastic damping component instead of both of them simultaneously. To incorporate the aeroelastic effect on flutter analysis, an integrated FE model, consisting of a particular structural element *e* and two fictitious *Matrix27* elements, was developed. As shown in Fig. 2, a pair of *Matrix27* elements was attached to each element *e* of the bridge beam to simulate the aeroelastic forces acting on the two nodes. The two *Matrix27* elements are separately plotted in the figure for clarity. Element *e*1 was employed to model aerodynamic stiffness, and element *e*2 was used to model aerodynamic damping. Element *e*, *e*1 and *e*2 share the same nodes, *i* and *j*.

Assembling all elemental matrices into global aeroelastic stiffness and damping matrices leads to:

$$\mathbf{F}_{ae} = \mathbf{K}_{ae}\mathbf{q} + \mathbf{C}_{ae}\dot{\mathbf{q}} \tag{6}$$

where $\mathbf{K}_{ae}$ and $\mathbf{C}_{ae}$ denote the global aeroelastic stiffness and damping matrices, respectively.

Substituting Eq. (6) into Eq. (1) results in the governing equations of motion for the bridge as:

$$\mathbf{M}\ddot{\mathbf{q}} + \left(\mathbf{C} - \mathbf{C}_{ae}\right)\dot{\mathbf{q}} + \left(\mathbf{K} - \mathbf{K}_{ae}\right)\mathbf{q} = \mathbf{0} \tag{7}$$

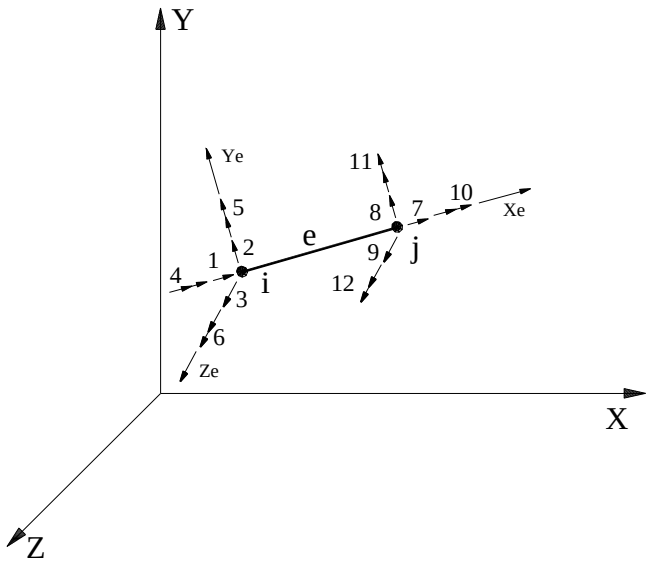

Fig. 1 Space frame element of member and global coordinate system

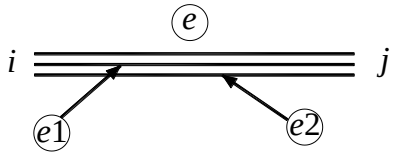

Fig. 2 Finite element model formulated in ANSYS to account for self-excited forces

After incorporating the Rayleigh structural damping matrix assumption $\mathbf{C}=\alpha\mathbf{M}+\beta\mathbf{K}$, the governing equations of motion for flutter analysis becomes

$$\mathbf{M}\ddot{\mathbf{q}}+\left(\bar{\mathbf{C}}-\bar{\mathbf{C}}_{ae}\right)\dot{\mathbf{q}}+\left(\mathbf{K}-\mathbf{K}_{ae}\right)\mathbf{q}=\mathbf{0} \tag{8}$$

where $\bar{\mathbf{C}}$ is the modified damping matrix and $\bar{\mathbf{C}}_{ae}$ is the modified aeroelastic damping matrix and they are expressed as

$$\bar{\mathbf{C}}=\alpha\mathbf{M}+\beta\left(\mathbf{K}-\mathbf{K}_{ae}\right) \tag{9}$$

$$\bar{\mathbf{C}}_{ae}=\mathbf{C}_{ae}-\beta\mathbf{K}_{ae} \tag{10}$$

in which α and β are the proportionality coefficients for Rayleigh damping which can be obtained by least squares fitting, as

$$\min_{\alpha,\beta}\sum_{i=1}^{m}\left(2\xi_i\omega_i-\alpha-\beta\omega_i^2\right)^2 \tag{11}$$

in which ξ_i is the damping ratio of the *i*th mode; and *m* is the total number of mode considered.

Eq. (8) represents an integrated system with the effect of aeroelasticity, parameterized in terms of wind velocity and response frequency. Eq. (8) can be solved by a damped complex eigenvalue. If the system has *n* DOFs, there will be *n* conjugate pairs of complex eigenvalues and eigenvectors. The *j*th conjugate pair of complex eigenvalues can be expressed as

$$\lambda_j=\sigma_j\pm i\omega_j \tag{12}$$

where $i=\sqrt{-1}$; σ_j and ω_j, the real part and the imaginary part of the *j*th conjugate pair of complex eigenvalues, respectively, are the damping and the vibrating frequency of the system, respectively.

The system is dynamically stable if the real part of all eigenvalues is negative and dynamically unstable if the real part of one or more eigenvalues is positive. At a certain wind velocity U_c, the real part becomes zero, which means the system is on the critical state. Correspondingly, ω_f is the flutter frequency and the wind velocity U_c is the critical flutter wind velocity.

As shown in Eq. (5), the aeroelastic stiffness and damping matrices in *Matrix27* elements are expressed in terms of three parameters, i.e., wind speed, circular frequency, and reduced frequency, but only two of them are independent. Thus a sweep and iterative procedure is needed to estimate the condition for occurrence of flutter instability. In this study, a mode-by-mode tracing method (Ge and Tanaka 2000) was adopted to iteratively search the flutter frequency and determine the critical flutter wind velocity. Making use of the tool APDL in ANSYS, the sweep and iterative procedure were implemented.

3. Description of Zhongdu Bridge over Yangtze River

The Zhongdu Bridge over Yangtze River, a three-span continuous suspension bridge, has a

main span of 600 m and a streamlined steel box girder with a width of 33 m and a height of 3 m. The two main cable planes are 26.7 m apart and the bridge deck is suspended by hangers at intervals of 12 m. The two bridge towers are high reinforced concrete structures with a height of 112.7 m and 107.6m, respectively. A sketch of the bridge is shown in Fig. 3. The material and sectional parameters of the bridge are shown in Table 1.

The finite element model of Zhongdu Bridge was established using ANSYS software. In the finite element model, the main girders and two towers were modeled by spatial beam elements with 6 degrees of freedom (DOF) at each node. The main cables and hangers were simulated spatial truss elements with 3 DOFs at each node, and the main cables were also meshed to match the nodes of hangers. The truss elements were assigned tension-only, and the nonlinearity if the back cable stiffness due to the gravity was approximated by using the equivalent modulus of elasticity (Ernst 1965). Wind tunnel tests have been conducted on an aeroelastic section model of the bridge (Chen 2013). The aerodynamic stability of the bridge in the final stage of the bridge was investigated and the flutter derivative parameters at the construction stage and the final stage all had been measured under the wind attack angles of -3^o, 0^o, and $+3^o$, as shown in Fig. 4.

The construction of the whole bridge was divided into 9 stages, with the corresponding percentages of deck completion being 9.8%, 21.8%, 33.8%, 45.8%, 57.8%, 65.8%, 77.8%, 89.8%, and 100% (final stage). The erection length and ratio of the stiffening girder at different construction stages are shown in Table 2. The actual sequence of deck erection for the Zhongdu Bridge is from the mid-span to the pylons and is symmetric, as shown in Fig. 5, which is defined as Sequence A. To investigate the effect of the sequence of deck erection on the evolution of dynamic properties and flutter stability limits through the deck erection stages, another two non-symmetric sequences of deck erection were studied, as shown in Figs. 6 and 7, which are defined as Sequence B and Sequence C, respectively.

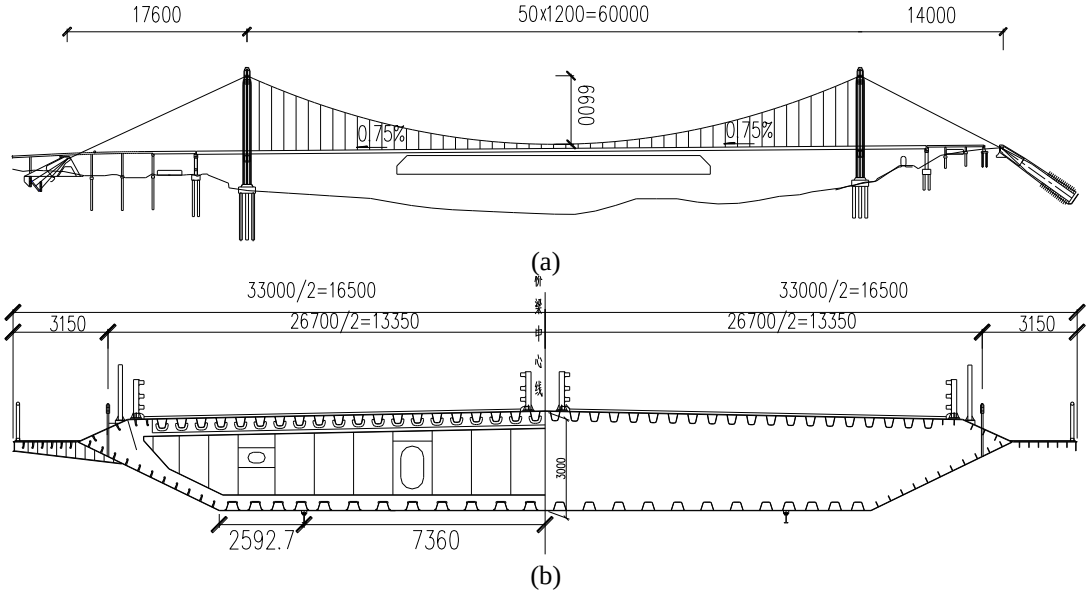

Fig. 3 The sketch of Zhongdu Bridge: (a) elevation view (unit: cm); (b) cross section (unit: mm)

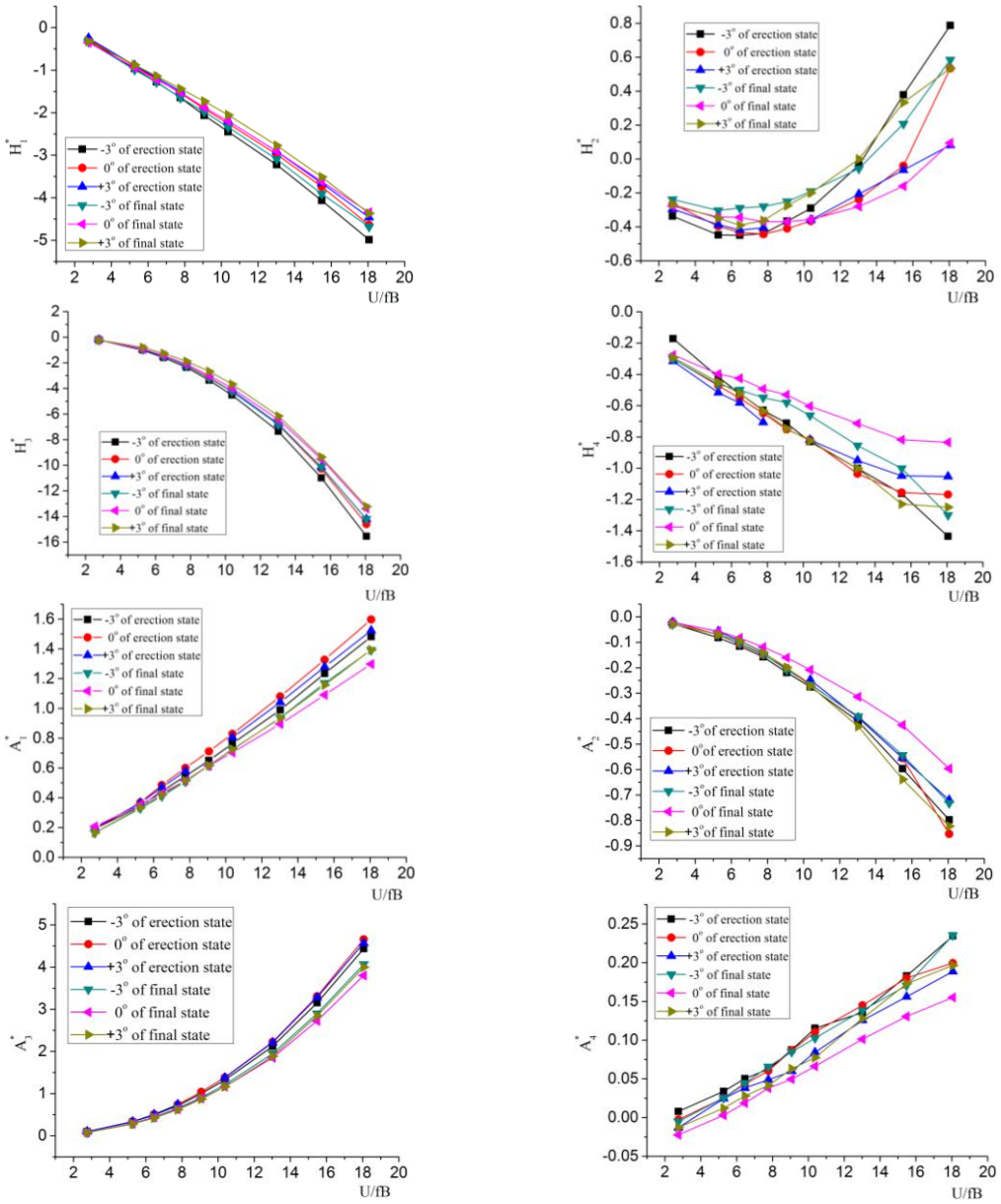

Fig. 4 The measured flutter derivatives

During the erection process of the suspension bridge, the stiffening girders will be connected with temporary hinges, as shown in Fig. 8, and will not be rigidly welded together until all segments are in position. From Fig. 8, it can be seen that the stiffening girder are just connected by the temporary hinges at the top flange plate, which means that the top flange plate is extruded and the bottom flange plate is separated during the erection process, which will result in the reduction of the girder stiffness, especially for the vertical bending stiffness (EI_z). Therefore, it is necessary

to investigate the effects of the stiffness reduction. Li *et al*. (2010) investigated the temporary connections of the stiffening girders of the long-span suspension bridge during erection by using three methods including beam simulating method, average stiffness method and temporary hinge method. In the present study, the average stiffness method was adopted to simulate the stiffness reduction of the girders during erection, in which the vertical bending stiffness (EI_z), the lateral bending (EI_y) stiffness and the torsional stiffness (EI_t) of the stiffening girder are reduced to 10%, 50% and 80% of the corresponding stiffness at the final state, respectively. It is noted that these reductions are rather empirical and used here to investigate and demonstrate their sensitivities for the bridge flutter behavior during the erection process. Since, as will be shown later, the flutter performance is not sensitive to the stiffness reduction during the construction process, a more accurate simulation of the stiffness reduction for a specific connection is not necessary.

Table 1 Material and sectional parameters of Zhongdu Bridge

Structural members	A (m^2)	J_θ (m^4)	J_y (m^4)	J_z (m^4)	E (GPa)	ρ (kg/m^3)
Main girder	1.31	5.13	1.93	102.00	210	15643
Main cables	0.1753	-	-	-	210	8000
Hangers	0.0031	-	-	-	210	8000
Towers	17.03-26.94	122.6-241.9	64.67-112.6	86.64-197.6	35	2650

Note: A-section area; J_θ-torsional moment of inertia; J_y-vertical bending moment of inertia; J_y-lateral bending moment of inertia; E- modulus of elasticity; ρ-density.

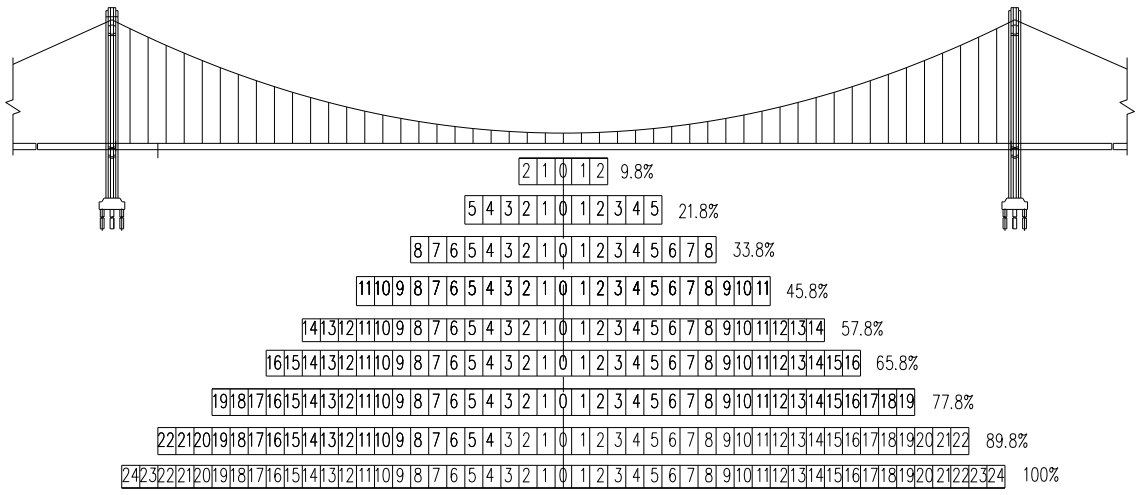

Fig. 5 Sequence A of deck erection

Table 2 Erection length and ratio of stiffing girder at different construction stages

Construction stage	1	2	3	4	5	6	7	8	9
Erection length (m)	59	131	203	275	347	395	467	539	600
Erection ratio (%)	9.8	21.8	33.8	45.8	57.8	65.8	77.8	89.8	100

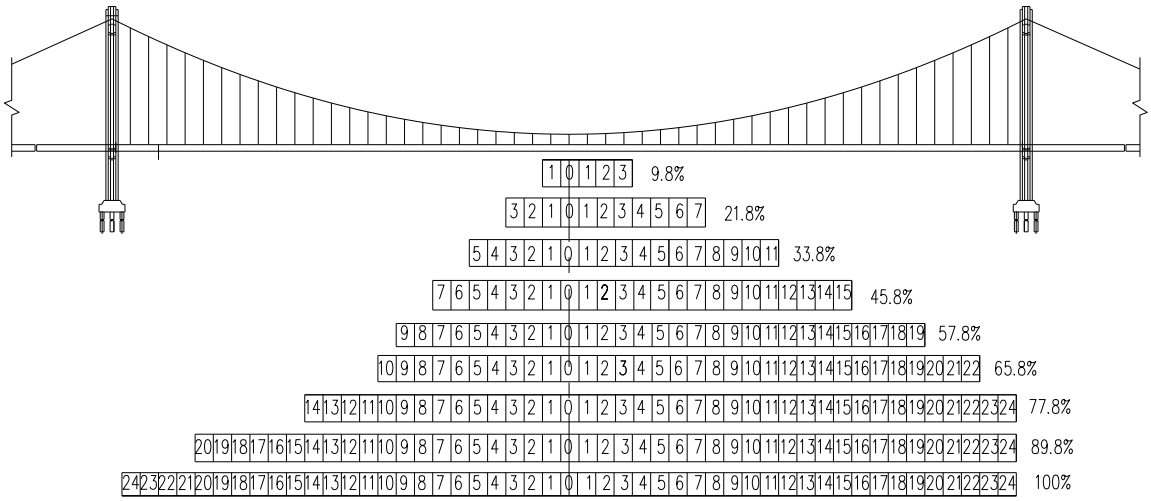

Fig. 6 Sequence B of deck erection

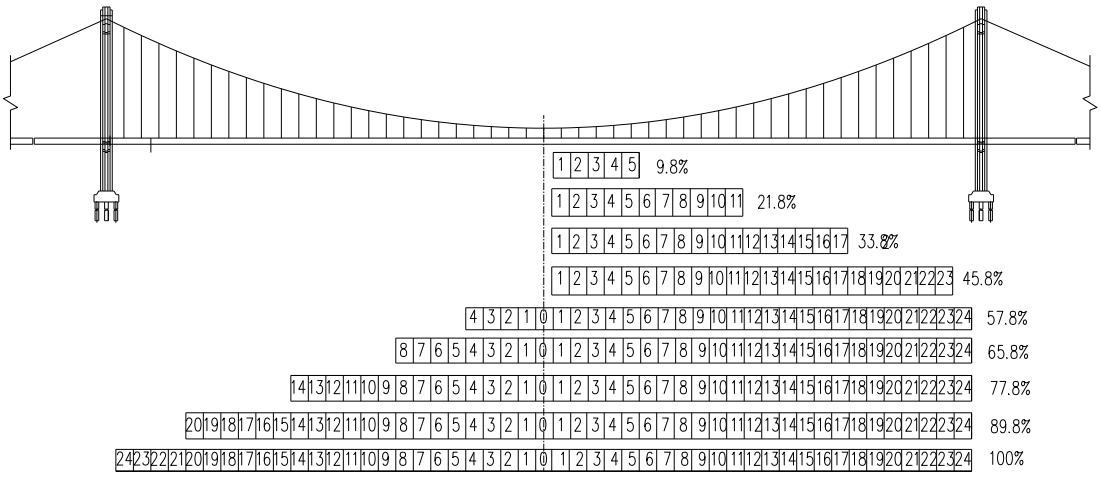

Fig. 7 Sequence C of deck erection

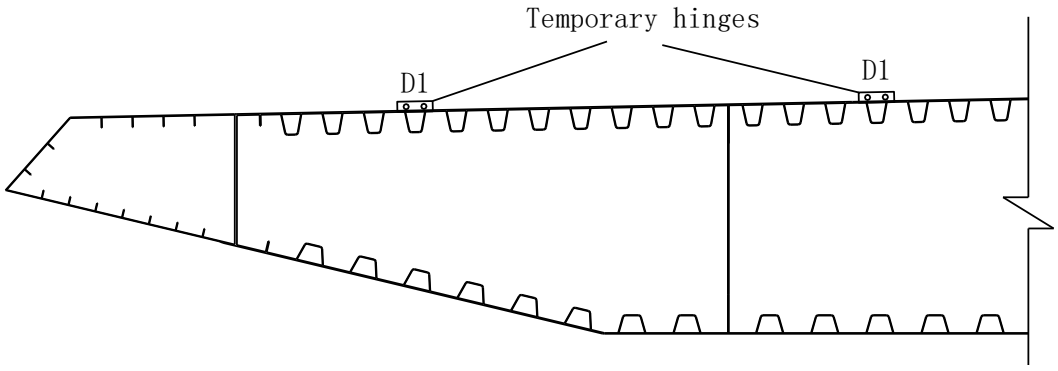

(a) The position of temporary hinges on the top flange plate

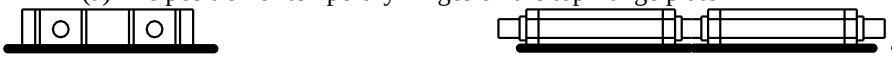

(b) Sketch of connection

Fig. 8 Temporary hinges during construction stage

4. Aerodynamic stability analysis of the bridge during erection

4.1 Effect of initial wind attack angle

For comparing with the testing results, the flutter wind speeds of the bridge in the final stage for -3°, 0°, 3° wind attack angles for Sequence A with the damping ratio of 0.5% were analyzed, as listed in Table 3. It can be seen that it is easier to induce the aerodynamic instability for +3° wind attack angle. The calculated results agree well with the test results, indicating that the method presented in this paper is credible.

The degree of participation for each mode shape during the deck erection was analyzed by using least squares fitting, as

$$\phi_f = \{\phi_1 \quad \phi_2 \quad \cdots \quad \phi_m\} \begin{Bmatrix} q_1 \\ q_2 \\ \cdots \\ q_m \end{Bmatrix} \tag{13}$$

in which ϕ_f is the actual vibration shape of flutter limit state of the bridge (or called flutter mode); ϕ_i (i=1 to m) is the ith mode shape of the bridge in stable state; and m is the total number of mode considered.

The results of flutter analysis of the bridge at different construction stages for Sequence A with the damping ratio of 0.0% under 0° wind attack angle are listed in Table 4. The first symmetric vertical bending and torsional frequencies for the different erection stages are shown in Fig. 9.

Table 3 Flutter wind speed of Zhongdu Bridge in the final stage with the damping ratio of 0.5%

Wind attack angle	-3°	0°	+3°
Calculated flutter speed (m/s)	151.5	145.3	142.8
Measured flutter speed (m/s)	152.8	146.2	143.4

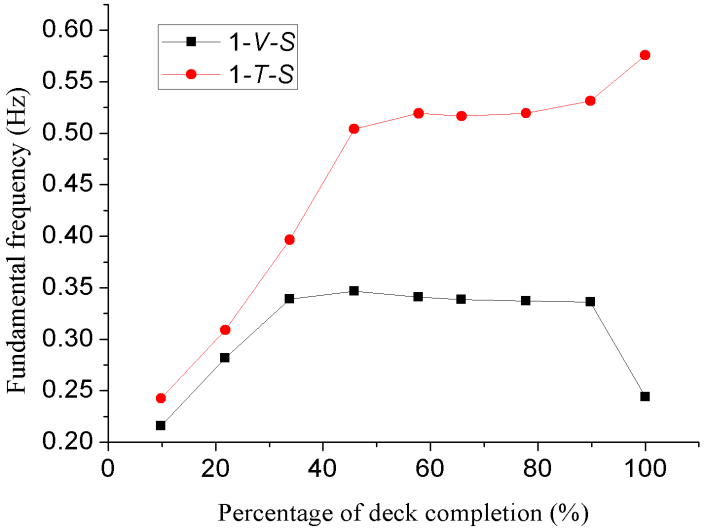

Fig. 9 The first symmetric vertical bending and torsional frequencies as erection proceeds

Table 4 Results of flutter analysis of Sequence A with the damping ratio of 0.0%

Construction stage (%)	Flutter speed ($m \cdot s^{-1}$)	Flutter frequency (Hz)	Main involved mode shape
9.8	39.1	0.2339	1-*S*-*V* 1-*S*-*T*
21.8	59.5	0.2999	1-*S*-*V* 1-*S*-*T*
33.8	69.6	0.3864	1-*S*-*V* 1-*S*-*T*
45.8	89.9	0.4524	1-*S*-*V* 1-*S*-*T*
57.8	92.0	0.4488	1-*S*-*V* 1-*S*-*T*
65.8	92.4	0.4466	1-*S*-*V* 1-*S*-*T*
77.8	94.1	0.4452	1-*S*-*V* 1-*S*-*T*
89.8	95.0	0.4619	1-*S*-*V* 1-*S*-*T*
100	134.8	0.4646	1-*S*-*V* 1-*S*-*T*

Note: *S*-symmetric; *V*-vertical bending; *T*-torsional.

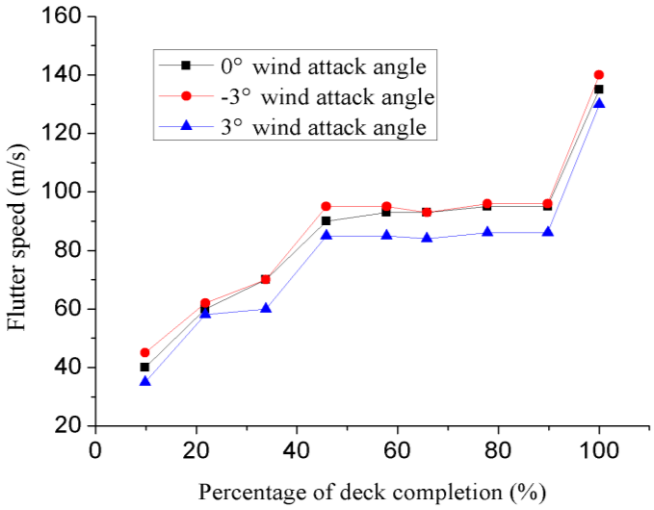

Fig. 10 Evolution of flutter speed under different initial wing attack angles

From Table 4, it can be seen that the minimum flutter speed occurs at the early erection stage and the flutter speed increases as the deck erection proceeds. The flutter mode is mainly contributed by the first symmetrical vertical bending and torsional mode shapes.

From Fig. 9, it can be found that both the first symmetric vertical bending and torsional frequencies increase gradually as erection proceeds from Stage 1 to Stage 4 (from 9.8% to 45.8%). The frequencies basically remain unchanged from Stage 4 to Stage 8 (from 45.8% to 89.8%), which results in the very little change of the flutter wind speed from Stage 4 to Stage 8, as shown in Table 4. There is a sudden decrease of the first symmetric vertical bending frequency at the final state (correspondingly an increase of the frequency ratio between the torsional and vertical mode), which contributes to the rapid increase of the flutter wind speed, as shown in Table 4. At the final stage, the side span girder is connected to the main span girder, all segments are rigidly welded together and supported by the cross girder of the tower at each ends. Therefore, there is a system transformation and a sudden increase of modal mass at the final state, which probably leads to the sudden decrease of the first symmetric vertical bending frequency.

In order to analyze the influence of the initial wind attack angle on flutter wind speed during erection, the aerodynamic stability analysis for -3^o, 0^o, $+3^o$ wind attack angles are performed considering the stiffness reduction with the damping ratio of 0.0% for Sequence A, with the results shown in Fig. 10. It can be seen that the initial wind attack angle of -3^o is advantageous for the aerodynamic stability, while the initial wind attack angle of $+3^o$ is disadvantageous for the aerodynamic stability, compared with the initial wind attack angle of 0^o during the deck erection.

4.2 Effect of sequence of deck erection

The symmetric sequence of deck erection (Sequence A, as shown in Fig. 5) and the two non-symmetric sequences of deck erection (Sequence B and C, as shown in Figs. 6 and 7) are analyzed to investigate the effect of sequence of deck erection on the evolution of dynamic properties and flutter stability limits through the deck erection stage, considering the stiffness reduction under 0^o wind attack angle with the damping ratio of 0.0%. The ratio of deck

eccentricity is defined as Δ/L_e, where Δ is the distance between the center of the erected deck and the midspan and L_e is the erected deck length. The deck eccentricity ratios of Stage 1 to Stage 4 of sequence B are between 0.17 and 0.2 and the deck eccentricity ratios of Stage 1 to Stage 4 of sequence C are from 0.52 to 0.59.

Fig. 11 shows the evolutions of the first symmetrical vertical bending and torsion frequencies of different construction sequences with different deck erection stages. It can be seen that the first torsional frequency increases obviously with the increase of eccentricity ratio from construction sequence A to C. The non-symmetrical erection sequence results in the increase of the frequency ratio between the first symmetric vertical bending and torsional frequencies, particularly at the early erection stages, as shown in Fig. 12.

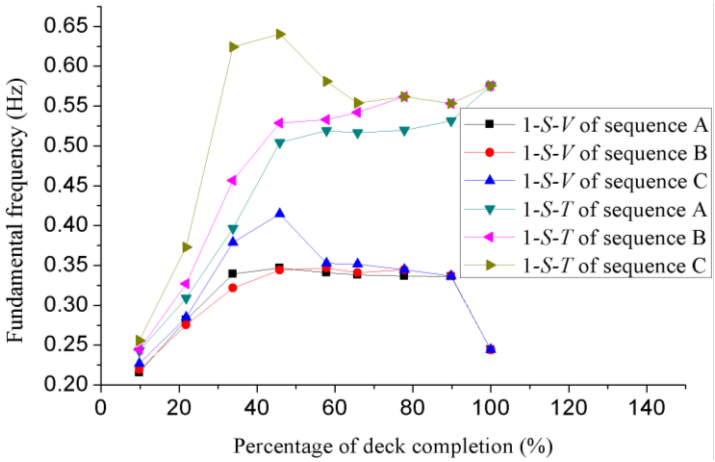

Fig. 11 The first symmetric vertical bending and torsional frequencies

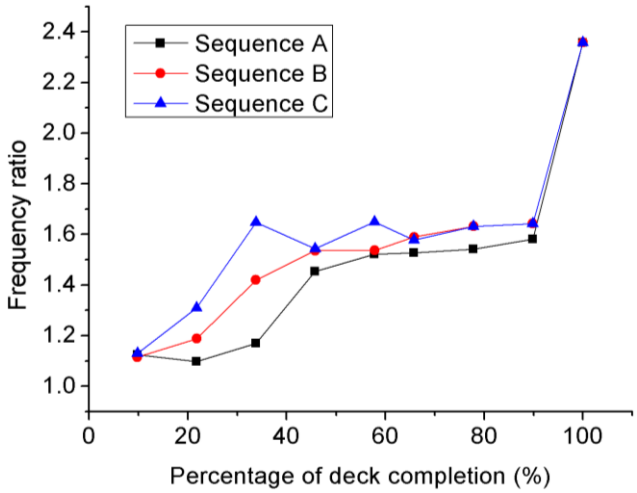

Fig.12 Frequency ratio of different erection frequencies of different erection sequence as erection proceeds sequence

Fig. 13 shows the evolutions of flutter wind speeds with the percentage of deck completion under different erection sequences. The first few stages from 9.8% to 45.8% of Fig. 13 are expanded in Fig. 14 to further examine the effect of eccentricity ratios on the flutter velocity.

From Fig. 13, it can be seen that the non-symmetrical erection sequences are favorable for the aerodynamic stability of long-span suspension bridges with a greater flutter wind speed than the symmetrical erection sequence. The increase is probably attributed to the increase of the torsional frequency for the non-symmetrical erection sequences, as shown in Fig. 11. Therefore, it is desirable to use a non-symmetrical erection sequence to improve the flutter stability of long-span suspension bridges during erection.

From Fig. 14, it is found that the flutter wind speed increases remarkably as the deck eccentricity ratio increases. However, the larger eccentricity ratio might generate geometry problems, as the movements of the cables are considerably larger from the initial stages to the final state. Thus, the best erection sequence should be investigated in the design phase of a long-span suspension bridge.

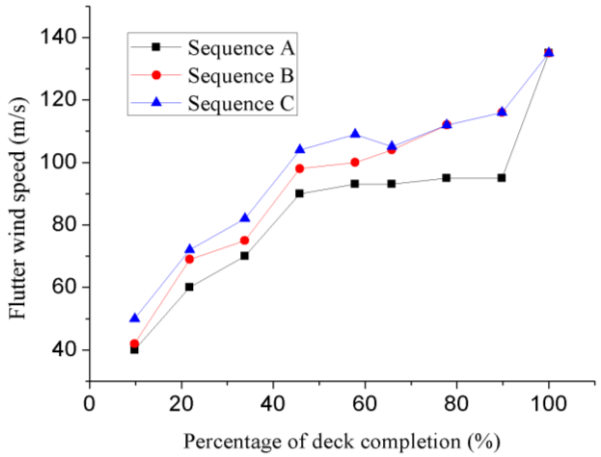

Fig. 13 Flutter wind speed of different erection sequences as erection proceeds

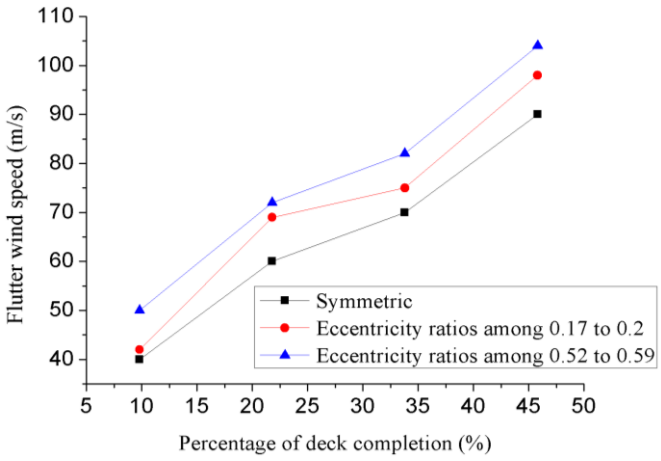

Fig. 14 Flutter wind speed of different eccentricity ratios

4.3 Effect of stiffness reduction of stiffening girder

For investigating the effect of stiffness reduction of the stiffening girder on the flutter wind speed during erection, the results of no reduction on the stiffness of the stiffening girder was compared with the results for the stiffness reduced, as shown in Fig. 15, under the condition of Sequence A, 0^{o} wind attack angle and damping ratio of 0.0%.

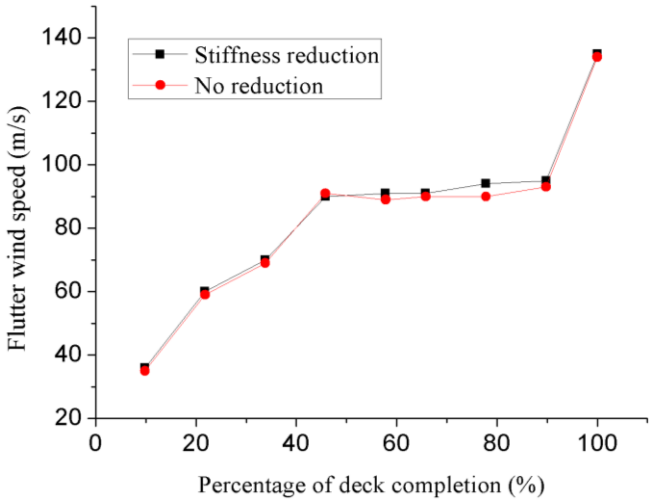

Fig. 15 Effect of stiffness reduction on flutter wind speed

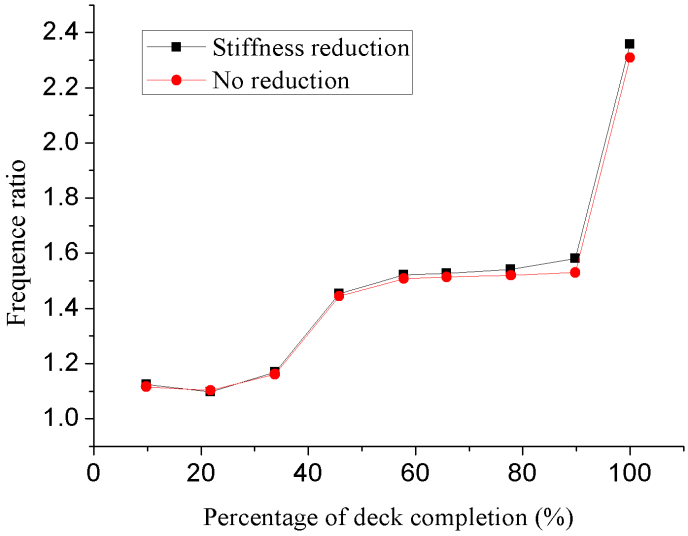

Fig. 16 Effect of stiffness reduction on frequency ratio of torsion and bending

Fig. 15 shows that stiffness reduction does not mean the decrease of the flutter speed. At the early erection stages, there is good agreement between the flutter wind speeds for stiffness reduction and no reduction. However, from Stage 5 to Stage 8, the flutter wind speeds for stiffness reduction are slightly higher than those with no reduction. This is probably due to that with the stiffness reduction described above, the first symmetrical torsion frequency basically remains unchanged and the first symmetrical vertical bending frequency slightly declines. This results in the slight increase of the frequency ratio between the torsional and vertical modes, as shown in Fig. 16, and contributes to the small increase of the flutter wind speed, as shown in Fig. 15.

4.4 Effect of structural damping

Structural damping is one of the most important parameters for the flutter stability of bridges (Cai *et al*. 1999b). When the damping of the whole system that is composed of structural damping and aerodynamic damping caused by self-excited forces changes from positive to zero, the vibration system is entering into a flutter critical state. To investigate the effect of structural damping on the flutter stability of the suspension bridge, damping ratios of 0.5%, 1% and 1.5% are selected for the flutter analysis with the results shown in Fig. 17, under the condition of Sequence A, stiffness reduction and 0^{o} wind attack angle.

It is shown in Fig. 17 that the greater the structural damping ratio, the higher the flutter wind speed, particularly at the early erection stages (from 9.8% to 33.8%). The flutter wind speed of Stage 2 (21.8%) increases remarkably up to 30.7% when the damping ratio increases from 1% to 1.5%. At the final state, the growth of the flutter wind speed is not obvious and the influence of damping ratio decreases significantly. The reason is, at the early erection stages, the stiffening girder is relatively short, and the structural damping is dominant in the whole system damping and has a great impact on the flutter wind speed. When the stiffening girder becomes longer, more energies are absorbed from wind loads and are turned into the aerodynamic damping, which consequently becomes larger. Thus, in the later construction stages, aerodynamic damping accounts for the most part of the whole system damping and directly influence the flutter stability of the structure, resulting in the lower importance for the structural damping.

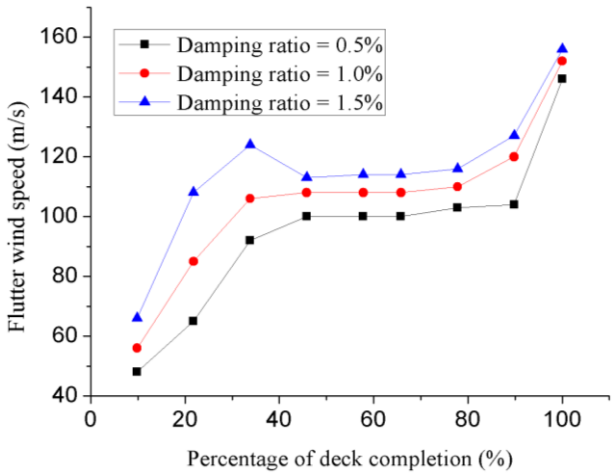

Fig. 17 Effect of damping ratio on flutter wind speed

4.5 Effects of cross cables

As is well known, during the erection stages, the structural stiffness of long-span suspension bridges mainly comes from the main cables, therefore, cross cables can be used to enhance the torsional stiffness and contribute to the flutter stability of long-span bridges. The effect of cross cables on the flutter stability were investigated in some previous studies (Yoneda *et al*. 1998, Cai *et al*. 1999, Li *et al*. 2012). In order to investigate the effect of cross cables on the flutter speed of the Zhongdu Bridge during construction, two kinds of cross cables were analyzed separately for Sequence A, the horizontal cross cables and the vertical cross cables, with the condition of the damping ratio of 0.5%, stiffness reduction, and 0^o wind attack angle. It is noted that, based on numerical investigations, the addition of these cross cables does not affect the participation of the natural modes in the flutter vibration shape.

4.5.1 Effect of the horizontal cross cables

The layout of the horizontal cross cables with the radius of 0.065 m was shown in Fig. 18, starting from the tower to the midspan, where △L is the length of the horizontal cross cables arranged along the span. During the erection process, the cross cables were arranged from the tower to the midspan symmetrically while lifting the stiffening girders. As listed in Table 5, three lengths of the horizontal cross cables arranged along the span were analyzed to investigate the influence of different lengths on the flutter speed of the bridge, with the results shown in Figs. 19. 20 shows the first symmetrical vertical and torsional frequencies of the three cases.

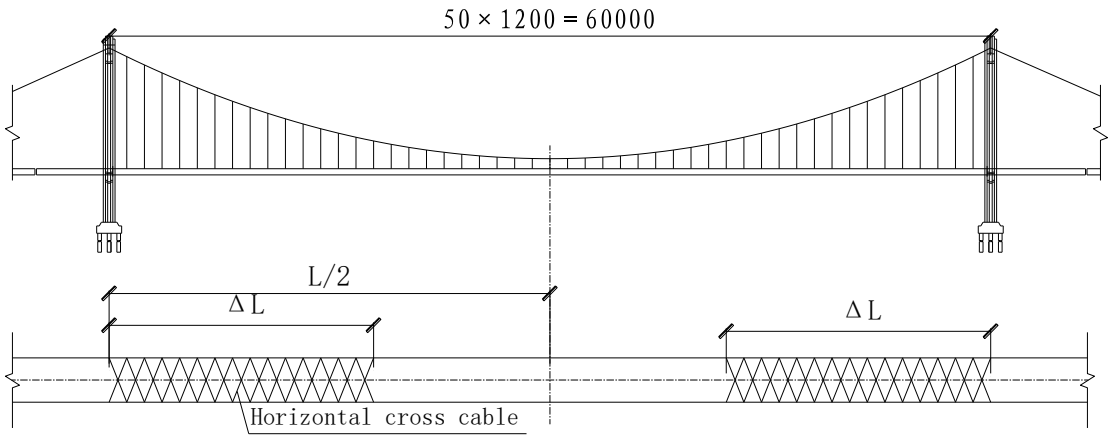

Fig. 18 Layout of horizontal cross cables

Table 5 Cases of horizontal cross cables arranged along the span

Cases	1	2	3
ΔL (m)	300	180	0
ΔL/L	0.5	0.3	0

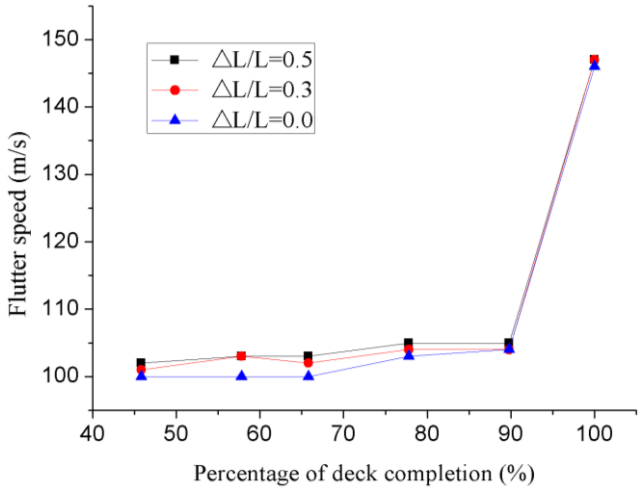

Fig. 19 Effect of horizontal cross cables on flutter wind speed

From Fig. 19, the flutter speed increases with the increase of the length of the horizontal cross cables arranged along the span; however, when the length is over 180 m, the increase of the length has a small influence on the flutter speed. From Fig. 20, the first symmetrical vertical frequency stays nearly unchanged with horizontal cross cables arranged along the span while the torsional frequency increases with the increase of the length of the horizontal cross cables arranged along the span. The first torsional mode shape of the bridge is a symmetrical, torsional vibration which means that the two main cables vibrate about the longitudinal axle of the bridge anti-symmetrically. The horizontal cross cables arranged on the two main cables will restrain this vibration of the two main cables, which results in the increase of the first torsional frequency and the flutter speed.

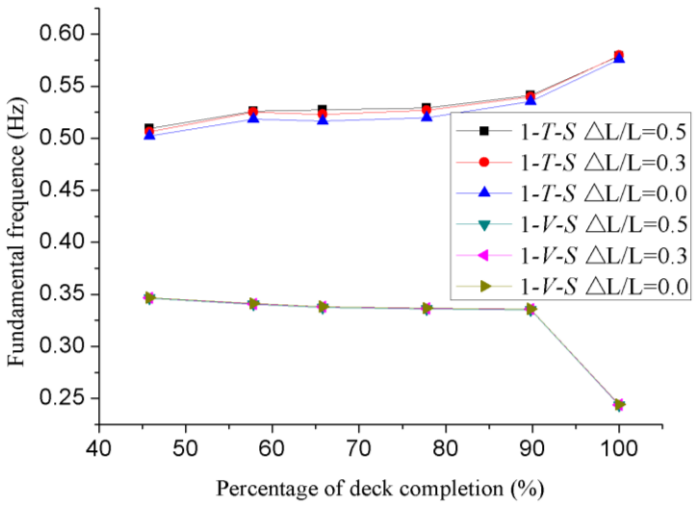

Fig. 20 Vertical and torsional fundamental frequencies with horizontal cross cables

4.5.2 Effect of the vertical cross cables

One pair of vertical cross cables with the radius of 0.065 m was arranged on the center span of the bridge symmetrically, as shown in Fig. 21, where ΔL is the distance from the location of the vertical cross cables to the tower. In order to investigate the effect of the location of the vertical cross cables on the flutter stability of the bridge, three cases were studied, as listed in Table 6. The vertical cross cables provide lateral connections between the main cable and the girder, enhancing the torsional stiffness of the bridge deck. It is noted that too many vertical cross cables may cause esthetic issues and may block traffic if they are too close to the mid-span for bridges in service. However, the vertical cross cables can be used as temporary bracing, and can be removed after completion of the construction.

Fig. 22 shows the evolution of flutter wind speeds with the percentage of deck completion for the three cases and comparing with the result of no cross cables. The results show that the flutter speeds for ΔL/L=0.36 are higher, but lower for ΔL/L=0.30 and 0.24 than the results of no cross cables from Stage 4 to Stage 8. According to this study, in order to improve the flutter stability of the bridge during erection, especially at the early stages, ΔL/L=0.36 is the best location of the vertical cross cables.

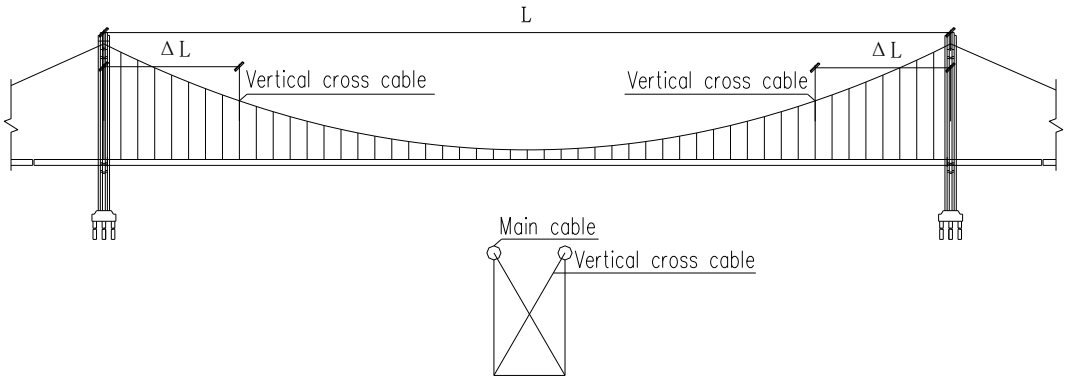

Fig. 21 Layout of vertical cross cables

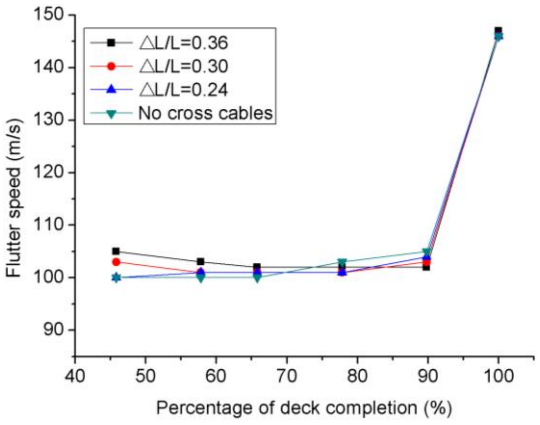

Fig. 22 Effect of vertical cross cables on flutter wind speed

Table 6 Cases of vertical cross cables

Cases	1	2	3
ΔL (m)	216	180	144
ΔL/L	0.36	0.3	0.24

5. Conclusions

Using the commercial FE package ANSYS, numerical flutter stability analyses, for the construction process of the Zhongdu Bridge over the Yangtze River, have been performed and the conclusions are summarized as follows:

(1) The flutter wind speed of long-span suspension bridges under construction is influenced by the erection sequence; a non-symmetrical erection sequence can enhance the flutter speed significantly. Particularly at the early erection stages, the flutter speed increases remarkably as the deck eccentricity ratio increases.

(2) The initial wind attack angle of -3^o is advantageous for the aerodynamic stability, but the initial wind attack angle of $+3^o$ is disadvantageous, compared with the initial wind attack angle of 0^o during the deck erection.

(3) The stiffness reduction of the stiffening girder has a slight effect on the flutter wind speed of the suspension bridge during erection.

(4) Increasing the structural damping can enhance the flutter speed considerably, particularly at the early stages.

Acknowledgements

The work described in this paper is supported by the key basic research project (973 project) of P.R. China, under contract No. 2015CB057706 and 2015CB057701. The authors would also like to gratefully acknowledge the supports from the National Science Foundation of China (Project 51278069; 51208067; 51178066). The work described in this paper is also supported by a special major project of the Western Transportation Program of Ministry of Transport of P.R. China, under contract No. 2011 318 824 140.

References

Brancaleoni, F. and Brotton, D.M. (1981), "Analysis and prevention of suspension bridge flutter in construction", *Earthq. Eng. Struct. D.*, **9**, 489-500.

Brancaleoni, F. (1992), "The construction phase and its aerodynamic issues", *Aerodynamics of Large Bridges*, Balkema, Rotterdam, FL, 147-158.

Cai, C.S., Albrecht, P. and Bosch, H.R. (1999a), "Flutter and buffeting analysis: finite element and RPE solution", *J. Bridge Eng. - ASCE*, **4**(3), 174-180.

Cai, C.S., Albrecht, P. and Bosch, H.R. (1999b), "Flutter and buffeting analysis: Luling and Dear Isle bridges", *J. Bridge Eng. - ASCE*, **4**(3), 181-188.

Chen Z.Q. and Han Y. (2007), "Study of the influence of aerodynamic force matrix and flutter derivatives on critical flutter state", *China J. Highway and Transport*, **20**(2), 51-56. (In Chinese)
Chen, Z.Q., Han, Y., Hua, X.G. and Luo, Y.Z. (2009), "Investigation on influence factors of buffeting response of bridges and its aeroelastic model verification for Xiaoguan Bridge", *Eng. Struct.*, **31**, 417-431.
Chen, Z.Q. (2013), *Wind-resistant research report of Zhongdu Bridge over Yangtse River*, Research Report of Hunan University, Changsha.
Cobo del Arco, D. and Aparicio, A.C. (2001), "Improving the wind stability of suspension bridges during construction", *J. Struct. Eng.- ASCE*, **127**(8), 869-875.
Ernst, H.J. (1965), "Der E-Modul von Seilen unter Berücksichtigung des Durchhangers", *Der Bauing*, **40**(2), 52-55 (in German).
Ge, Y.J. and Tanaka, H. (2000), "Aerodynamic stability of long-span suspension bridges under erection", *J. Struct. Eng.- ASCE*, **126**(12), 1404-1412.
Hua, X.G., Chen, Z.Q., Ni, Y.Q. and Ko, J.M. (2007), "Flutter analysis of long-span bridges using ANSYS", *Wind Struc*t., **10**(1), 61-82.
Han Y. (2007), *Study on complex aerodynamic admittance functions and refined analysis of buffeting response of bridges*, *Ph.D. thesis*. China: Hunan University.
Jain, A., Jones, N.P. and Scanlan, R.H. (1996), "Coupled flutter and buffeting analysis of long-span bridges", *J. Struct. Eng. - ASCE*, **122**, 716-725.
Larsen, A. (1993), "Aerodynamic aspects of the final design of the 1624m suspension bridge across the Great Belt", *J. Wind Eng. Ind. Aerod.*, Amsterdam, **48**, 261-285.
Larsen, A. (1995), "Prediction of aeroelastic stability of suspension bridges during erection", *Proceedings of the 9th Int. Conf. on Wind Engrg.*, New Delhi, India.
Li, Y.L., Hou, G.Y., Li, C.J. and Qiang, S.Z. (2012), "Flutter stability of a super-long-span suspension bridge with CFRP main cables during erection", *J. Vib. Shock*, **31**(21), 15-21. (in Chinese)
Li, Y.L., Hou, G.Y., Cao, P.H. and Wang, T. (2010). "Finite element simulation of temporary connection between stiffening girder segments during erection for long-span suspension bridges", *Sciencepaper Online*, 5(7), 529-534.
Namini, A.H. (1991), "Analytical modeling of flutter derivatives as finite elements", *Comput. Struct.*, **41**, 1055-1064.
Scanlan, R.H. (1978), "Action of flexible bridges under wind, I: flutter theory", *J. Sound Vib.*, **60**(2), 187-199.
Tanaka, H., Damsgaard, A., Reino, P., Franck, N. and Madsen, B.S. (1996), "Aerodynamic stability of a suspension bridge with a partially constructed bridge deck", *Proceedings of the 15th Int. Assn. (*association*) of Bridge and Struct. Engrs. Congr. Rep.*, IABSE, Zurich.
Tanaka, H. and Gimsing, N.J. (1999), "Aerodynamic stability of non-symmetrically erected suspension bridge girders", *J. Wind Eng. Ind. Aerod.*, **80**, 85-104.
Yoneda, M., Ohno, K. and Tamaki, Y. (1998), "Best cross stay location for super long span suspension bridge", http://dx.doi.org/10.5169/seals-59919.
Zhang, X.J. (2004), "Investigation on aerodynamic stability of long-span suspension bridges under erection", *J. Wind Eng. Ind. Aerod.*, **92**, 1-8.

JH